processes

MDPI

Article

Determination of Basalt Fiber Reinforcement in Kaolin Clay: Experimental and Neural Network-Based Analysis of Liquid Limit, Plastic Limit, and Unconfined Compressive Strength

Yasemin Aslan Topçuoğlu [1], Zeynep Bala Duranay [2,*], Zülfü Gürocak [1] and Hanifi Güldemir [2]

[1] Department of Geological Engineering, Firat University, Elazığ 23119, Türkiye; yaslan@firat.edu.tr (Y.A.T.); zgurocak@firat.edu.tr (Z.G.)
[2] Electrical Electronics Engineering Department, Technology Faculty, Firat University, Elazig 23119, Türkiye; hguldemir@firat.edu.tr
* Correspondence: zbduranay@firat.edu.tr

Abstract: The use of basalt fibers, which are employed in various fields, such as construction, automotive, chemical, and petrochemical industries, the sports industry, and energy engineering, is also increasingly common in soil reinforcement studies, another application area of geotechnical engineering, alongside their use in concrete. With this growing application, scientific studies on soil reinforcement with basalt fiber have also gained momentum. This study establishes the effects of basalt fiber on the liquid limit, plastic limit, and strength properties of soils, and the relationships among the liquid limit, plastic limit, and unconfined compressive strength of the soil. For this purpose, 12 mm basalt fiber was used as a reinforcement material in kaolin clay at ratios of 1.0%, 1.5%, 2.0%, 2.5%, and 3.0%. The prepared samples were subjected to liquid limit, plastic limit, and unconfined compressive strength tests. As a result of the experimental studies, the fiber ratio that provided the best improvement in the soil properties was determined, and the relationships among the liquid limit, plastic limit, and unconfined compressive strength were established. The experimental results were then used as input data for an artificial intelligence model. The used neural network (NN) was trained to obtain basalt fiber-to-kaolin ratios based on the liquid limit, plastic limit, and unconfined compressive strength. This model enabled the prediction of the fiber ratio that provides the maximum improvement in the liquid limit, plastic limit, and compressive strength without the need for experiments. The NN results were in great agreement with the experimental results, demonstrating that the fiber ratio providing the maximum improvement in the soil properties can be identified using the NN model without requiring experimental studies. Moreover, the performance and reliability of the NN model were evaluated using 5-fold cross-validation and compared with other AI methods. The ANN model demonstrated superior predictive accuracy, achieving the highest correlation coefficient (R = 0.82), outperforming the other models in terms of both accuracy and reliability.

Keywords: artificial intelligence; basalt fiber; liquid limit; plastic limit; kaolin clay; neural network; soil reinforcement; unconfined compressive strength

Academic Editors: Navid Aslfattahi, Kumaran Kadirgama, Lingenthiran Samylingam and Mohammad Reza Chalak Qazani

Received: 26 December 2024
Revised: 27 January 2025
Accepted: 28 January 2025
Published: 30 January 2025

Citation: Topçuoğlu, Y.A.; Duranay, Z.B.; Gürocak, Z.; Güldemir, H. Determination of Basalt Fiber Reinforcement in Kaolin Clay: Experimental and Neural Network-Based Analysis of Liquid Limit, Plastic Limit, and Unconfined Compressive Strength. *Processes* **2025**, *13*, 377. https://doi.org/10.3390/pr13020377

1. Introduction

The primary principle of successful fill work is the use of soil that possesses the desired engineering properties for the fill. However, accessing such soils is not always possible. In such cases, improving the engineering properties of the soil to be used and rendering it suitable for fill applications becomes crucial. Since historical times, various types of additives with distinct characteristics have been added to soils to achieve chemical stabilization. Materials such as slaked lime, silica fume, fly ash, lime, volcanic ash, and tuff, which continue to be used today, induce pozzolanic reactions in soil, thereby ensuring its chemical stabilization. In recent years, the increasing use of fibers with different properties in automotive, construction, and mechanical engineering applications has led to numerous studies [1–3] on their physical, mechanical, chemical, and elastic properties. Additionally, fibers have begun to be used as an alternative to chemical stabilization in soil reinforcement applications.

Fiber reinforcement involves adding different types of fibers, such as carbon, polypropylene, and glass, to soil, enhancing the strength of clayey soils. As the use of fibers in soil reinforcement has become more widespread, the number of scientific studies in this field has also increased [4–15]. In addition to these fiber types, basalt fiber (BF), a relatively new type of fiber, has been incorporated into soil reinforcement applications in recent years. BF has a high modulus of elasticity and excellent heat resistance. It possesses a significant acoustic resistance capacity and is an outstanding vibration isolator. Additionally, it exhibits high corrosion resistance and is biologically stable and chemically inert [16]. With these properties, it can be considered a green and sustainable material. Compared to glass, carbon, or mineral fibers, BF has a lower environmental impact. Due to its high rigidity and low elongation at break, BF has attracted the attention of material scientists as a potential substitute for steel and carbon fibers [17]. These properties have also led to its growing importance in soil reinforcement applications in recent years. Derived from basalt rock, which is abundantly available, BF has become increasingly preferred over other fiber types due to its economic and natural properties, eco-friendliness, sustainability, and high tensile strength. Studies investigating the effects of BF on the engineering properties of soils have examined changes in the liquid limit (LL), plastic limit (PL), permeability, compressibility, and strength of various soils reinforced with BF. Numerous studies have been conducted to explore the effects of BF on soil strength [18–23].

In these studies, the optimum BF length and ratios that provide the highest strength in different types of soils have been investigated. For instance, Gao et al. [18] reported the optimum BF length as 12 mm and the optimum ratio as 0.25%. Gürocak and Aslan Topçuoğlu [21] achieved the maximum unconfined compressive strength (q_u) in low-plasticity kaolin clay (K) using 1% BF-reinforced samples prepared with 25% water content. Ndepete and Sert [24] indicated that when using 24 mm long BF, the optimum ratio should be 1.5%. Ocakbaşı [25] stated that in highly plastic clay, the maximum strength values were observed in mixtures prepared with a 24 mm BF length at a ratio of 2.0%.

Although there are numerous studies examining the changes in the strength of clayey soils after BF reinforcement, studies investigating the changes in the consistency of BF-reinforced clayey soils are relatively limited. Aravalli et al. [26] stated that when 12 mm long BF is used in clayey soils, an increase in the BF content leads to decreases in the LL, PL, and plasticity index (PI) values, making the soil less plastic. According to the researchers, during the LL test, the static forces in the BF are converted into frictional forces as a result of the impacts generated. This creates resistance against the sliding and flowing of the soil, thereby reducing the consistency limits of the soil. In the study conducted by Chaudhary [27], it was determined that the LL values of clayey soil reinforced with 3%, 6%, 9%, 12%, and 15% BF decreased up to a 9% BF content and increased thereafter, while the PL values increased up to a 12% BF content and then decreased. The researcher explained that the reduction in the LL was due to the tendency of the fibers to absorb water or moisture from the soil, thereby making the soil more stable. Khudhair et al. [28] reinforced low-plasticity clayey soil with BF and cement, finding that as the BF content increased, the

LL decreased, the PL increased, and consequently, the PI decreased, making the soil less plastic. Mukhtar and Kumar [29] observed that in clayey soil reinforced with 12 mm BF, the LL, PL, and PI values decreased as the BF content increased. They attributed these reductions to the transformation of static forces in BF into frictional forces during the LL test impacts. This friction makes the soil more resistant to sliding and flowing. Aishwarya and Priya Rachel [30] noted that in sandy clay soil reinforced with BF, the LL and PL values increased with increasing BF content, resulting in a decrease in the PI. Numerous similar studies in the literature can be found where the experimental results are evaluated using traditional statistical methods.

However, utilizing various advanced intelligent methods, such as artificial neural networks (ANN), genetic algorithms, fuzzy logic, and particle swarm optimization, to evaluate existing experimental data has become increasingly important in recent years. This approach not only demonstrates the applicability of new evaluation methods in geotechnical studies but also provides an opportunity to compare the results obtained from intelligent systems with those derived from traditional methods. A limited number of researchers [31–37] have evaluated the changes in the engineering properties of fiber-reinforced soils using intelligent methods. In the study by Armaghani et al. [31], the increase in strength was determined by using polypropylene fibers of different lengths and ratios in sandy soil. Hybrid ANN-based models, namely genetic algorithm (GA)-ANN and particle swarm optimization (PSO)-ANN, were used in the study to predict the shear strength parameters of the soil. It was stated that the GA-ANN model could provide a new feasible model for effectively predicting the cohesion of fiber-reinforced sandy soil. In the study by Garg et al. [32], models were developed using an extreme learning machine (ELM) to calculate the compressive strength of soil reinforced with different fiber types, such as coconut, jute, water hyacinth, and polypropylene. According to the study's results, the predictive accuracy of the ELM models appears to be sufficiently reasonable for estimating the compressive strength of fiber-reinforced soil. In the study conducted by Tiwari and Satyam [33], the effects of pond ash and polypropylene fibers on soil strength were investigated, and experimental data were analyzed using an ANN. The results of the ANN modeling demonstrated an excellent prediction of the mechanical properties. In the study conducted by Gül and Bashir [34], changes in the strength of glass fiber-reinforced soil were determined. An ANN was used to develop a model to predict the relationship between the soil strength and various reinforcement parameters. It was stated that the developed ANN could assist researchers in achieving the optimal fiber reinforcement ratio for a specific type of soil. Sungur et al. [35] aimed to predict the shear strength of clayey soil reinforced with glass fibers using an adaptive neuro-fuzzy inference system (ANFIS). Analyzing the statistical parameters revealed that the data split of 80% for training and 20% for testing yielded the most accurate results in shear strength prediction using the ANFIS model. In the study conducted by Sert et al. [36], BFs of different lengths were mixed with clay at different ratios, and their strengths were determined. The obtained dataset was used to train machine learning algorithms. The results demonstrated that decision tree (DT) regression provided the best performance in predicting stress and deformation.

1.1. Contributions of This Study

In this study, the effects of BF on the LL, PL, and strength properties of soils in geotechnical engineering were investigated. For this purpose, mixtures of K and BF in various proportions were prepared, and the prepared samples were subjected to LL, PL, and q_u tests to determine their soil properties.

The experimental results obtained from these tests were utilized as input data for an artificial intelligence (AI) model. The relationships among the LL, PL, and q_u in soils are inherently nonlinear and influenced by multiple interdependent factors. The neural network (NN) approach was chosen for this study due to its ability to model complex and nonlinear relationships among variables, which is particularly important in geotechnical engineering applications. Traditional statistical or analytical methods often struggle to accurately capture these intricate interactions, whereas NNs are well-suited for identifying patterns and relationships within complex datasets.

A review of the literature reveals that there are limited studies evaluating the changes in the strength, LL, and PL of clayey soils reinforced with different fiber types using AI techniques. Moreover, while various fiber types have been used in these studies, no research has evaluated the results of clayey soils reinforced with BF using AI methods. Therefore, there is a lack of a practical and efficient model for accurately predicting these improvements. Developing a model capable of predicting the optimal BF ratios to achieve the best results without conducting experimental studies, using an AI-supported approach, aims to fill a significant gap in the current literature.

1.2. Research Purpose

The primary objective of this research is to address the identified gap in the literature by providing an AI-driven solution for predicting the optimal BF ratios required to improve soil properties. Specifically, the study seeks the following:

- Determine the effects of 12 mm BFs on the LL, PL, and q_u properties of soils.
- Examine the relationships among the LL, PL, and q_u.
- Identify the optimal fiber ratio that provides the best improvement in soil properties by using different ratios of BF in K.
- Develop an NN model using experimental data to predict the optimal BF ratio based on the LL, PL, and q_u values.
- Demonstrate the accuracy of the NN model in predicting the fiber ratio that optimally enhances soil properties without experimental studies.

1.3. Innovative Aspects

This study introduces a novel approach distinct from those commonly observed in the literature. Instead of predicting the strength obtained from experimental studies based on predefined mixture ratios, this research focuses on estimating the mixture ratios required to achieve specified values of strength, LL, and PL. This reverse methodology offers a practical and efficient way to optimize soil properties without requiring additional experimental studies.

Moreover, this study demonstrates the application of AI, specifically NN, in geotechnical engineering, bridging the gap between experimental and computational methods. By doing so, it provides a sustainable and eco-friendly solution for soil stabilization using BF, which is naturally abundant and cost-effective.

2. Materials and Methods

In laboratory studies, kaolin, a clay type composed of aluminum hydrosilicate ($Al_2Si_2O_5(OH)_4$) formed through the in situ weathering of volcanic/magmatic rocks, was chosen. K produced from the kaolin quarry in Balıkesir—Sındırgı (Türkiye) was used (Figure 1a). As the reinforcing material, 12 mm long BF produced from dark-colored, fine-grained volcanic rock was employed (Figure 1b).

BF is a continuous filament produced by melting basalt rock at 1450 to 1500 degrees Celsius and drawing it through a bushing made of a platinum rhodium alloy [38]. The chemical composition of BF includes SiO_2, Al_2O_3, Fe_2O_3, MgO, CaO, Na_2O, and TiO_2 [39]. Depending on the tensile conditions, the tensile strength of pure BF ranges between 2 and

4 GPa [40]. The mechanical and physical properties of the BF used in the experimental studies were obtained from the company from which the BF was purchased and are presented in Table 1.

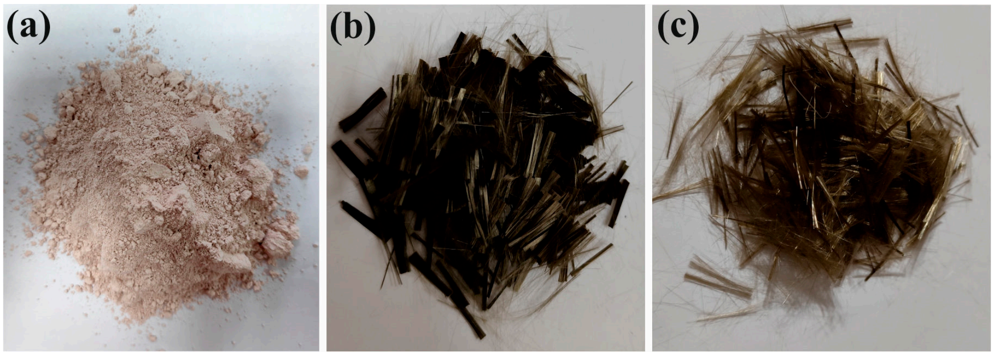

Figure 1. Used in experimental studies: (**a**) K; (**b**) unseparated BF; (**c**) BF separated by compressor.

Table 1. Physical and mechanical properties of BF.

Feature	Value
Length fiber	12 mm
Diameter of monofilament	15 ± 1.5 µm
Humidity	Max 2%
Modulus of elasticity	90 GPa
Tensile strength	3000 MPa
Thermal conductivity	0.031–0.038 W/mK
Elongation at break	3.5%
Density	2.63 g/cm^3

2.1. Laboratory Studies

The experimental studies consisted of stages, including preparation of the samples, determination of the LL and PL values, and conducting standard Proctor and unconfined compression tests. All experiments were carried out at Firat University, Department of Geological Engineering, Rock—Soil Mechanics Laboratory. The LL and PL values of the unreinforced clay were found to be 45.00% and 24.00%, respectively, with a PI value of 21.00%, [21] a w_{opt} value of 25%, and a γ_{dmax} value of 13.01 kN/m³ [23]. In the classification, kaolin was categorized as low-plasticity (CL) clay according to the Unified Soil Classification System (USCS) [21]. The geotechnical properties of the unreinforced clay used in the study are shown in Table 2.

Table 2. Geotechnical properties of unreinforced clay used in the study [21,23].

Properties	**LL (%)**	**PL (%)**	**PI (%)**	**Soil Class**	w_{opt} **(%)**	γ_{dmax} **(kN/m³)**
Values	45	24	21	CL	25	13.01

During the preparation of the reinforced clay samples, K dried in an oven at 105 °C for 24 h was mixed with BF separated by a compressor (Figure 1c) at the following percentages: 1.0%, 1.5%, 2.0%, 2.5%, and 3.0% by dry weight. LL and PL tests were conducted according to the ASTM D4318-17e1 standard [41] to determine the LL and PL values of the samples (Figure 2a–c). The LL values of the reinforced samples ranged from 38.80% to 42.30%, the PL values ranged from 26.00% to 28.00%, and the PI values ranged from 10.80% to 16.30%. All test results are presented in Table 3.

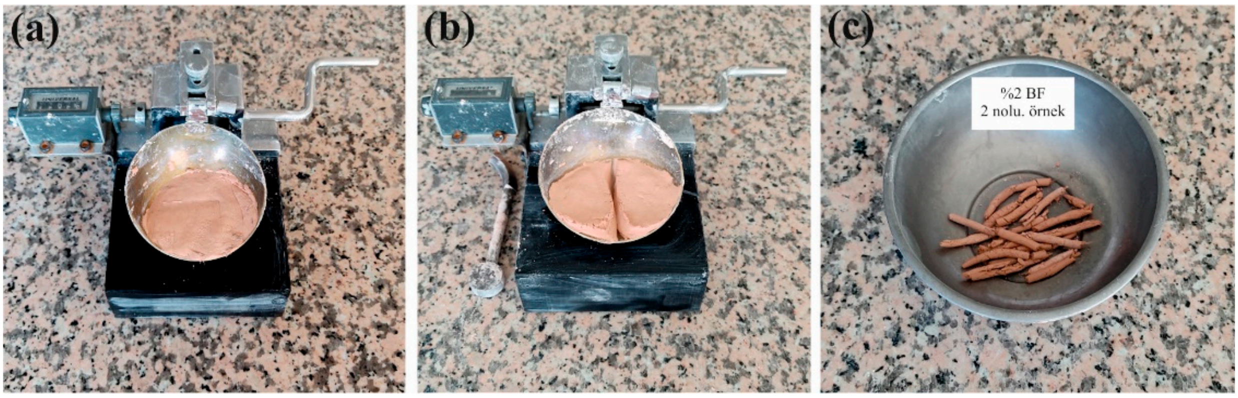

Figure 2. (**a**,**b**) Conducting the liquid limit test; (**c**) conducting the plastic limit test.

Table 3. The LL, PL, PI, and q_u values of the samples.

Samples	LL (%)	PL (%)	PI (%)	q_u (kPa)
K	45.00	24.00	21.00	294.08
K + 1.0% BF	40.50	26.40	14.10	767.95
K + 1.5% BF	40.20	27.70	12.50	829.11
K + 2.0% BF	38.80	28.00	10.80	949.06
K + 2.5% BF	39.50	27.41	12.09	905.60
K + 3.0% BF	42.30	26.00	16.30	800.77

K: kaolin clay; **LL:** liquid limit; **PL:** plastic limit; **PI:** plasticity index; **q_u:** unconfined compressive strength.

To ensure a homogeneous distribution of the BF within the clay during the preparation of the reinforced clay samples for unconfined compression tests, mixing was performed using a mixer and by hand (Figure 3a). The prepared mixtures were compacted at their w_{opt} using the standard Proctor test according to the ASTM D698-12e2 standard [42] (Figure 3b), and cylindrical specimens for unconfined compression tests were extracted from the compacted samples.

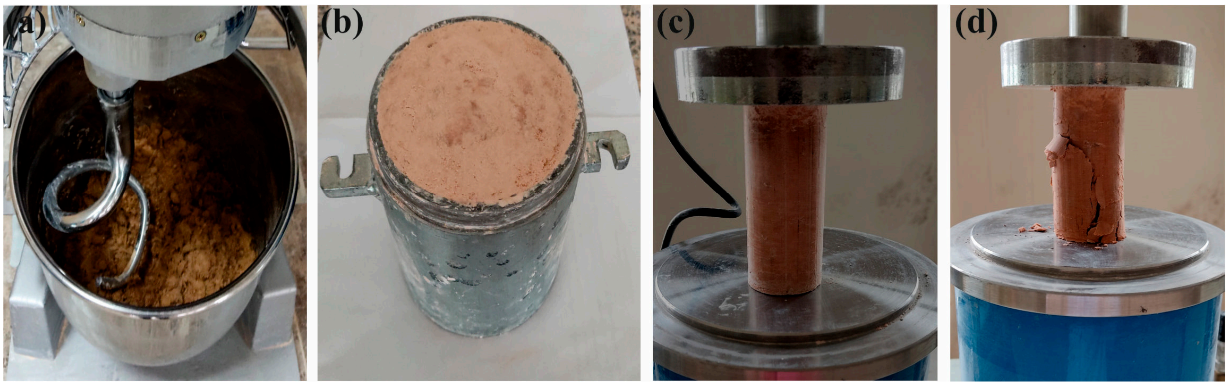

Figure 3. (**a**) Mixing of clay and BF samples with a mixer; (**b**) compacted sample with compaction test; (**c**,**d**) sample before and after unconfined compression test.

In the final stage of the experimental studies, unconfined compression tests were conducted on 30 samples according to the ASTM D2166M-16 standard [43], and the q_u values were calculated. The test was performed on cylindrical specimens with a height of 76 mm and a diameter of 38 mm, prepared from mixtures compacted in a Proctor mold (Figure 3c,d). The q_u values for all samples are presented in Table 3.

2.2. Neural Network

AI is a multidisciplinary field focused on enhancing the ability of computers to perform tasks such as learning, problem-solving, and decision-making by replicating human cognitive abilities [44]. AI is widely applied in various sectors, including healthcare, defense, energy, and engineering [45–49]. Commonly utilized AI techniques include NN, linear regression (LR), support vector machines (SVM), and Gaussian process regression (GPR). In this study, the experimental data were processed through multiple AI algorithms, with the NN being identified as the most efficient model.

NNs are sophisticated computational tools designed to emulate the structure and behavior of biological neural systems [50]. These networks interpret input data and produce optimal outputs based on predefined criteria, making them highly effective in tackling nonlinear challenges.

Figure 4 illustrates the core elements of the NN system used in this study. These included the input layer, hidden layer, and output layer. The input layer serves as the starting point, receiving the input data. The data are then processed in the hidden layer, which acts as an intermediary, applying weights to the input data to uncover complex patterns. Finally, the output layer provides the predictions according to the input data.

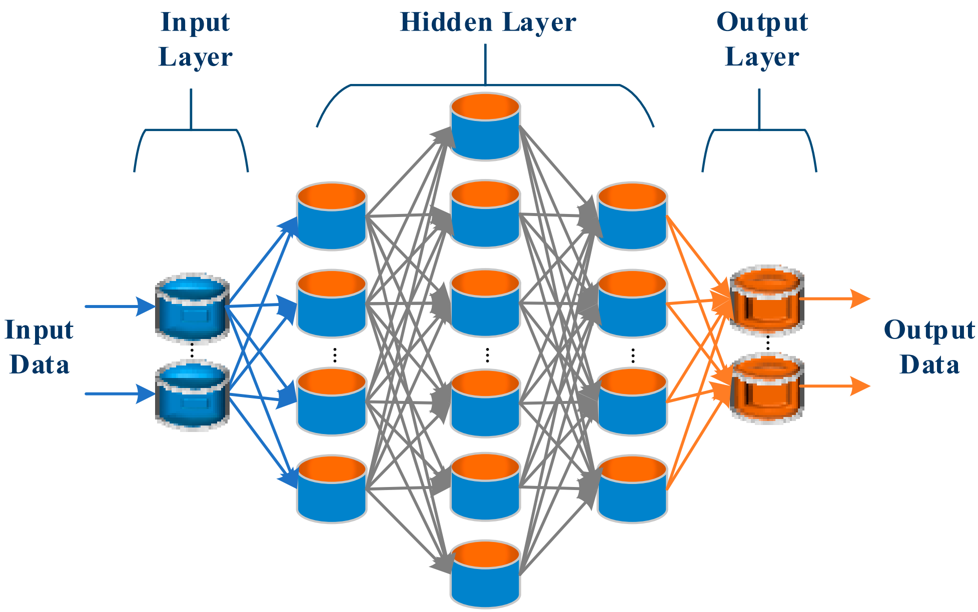

Figure 4. Core elements of NN system.

In this study, a single hidden layer was employed, as it was sufficient to model the relationships between the input and output variables. The architecture was optimized to achieve a balance between the learning capacity and computational efficiency. Figure 4 also shows the connections between these layers, emphasizing the flow of information from the input to the output layer through the hidden layer.

Training the NN model involves dividing the input data into subsets for training, testing, and validation. These subsets are used to fine-tune the network through various optimization algorithms, enabling the system to effectively capture the relationships between the inputs and outputs. With their inherent nonlinear capabilities, high memory efficiency, and rapid processing speeds, NNs provide a powerful approach to addressing complex computational problems.

Figure 5 represents the fundamental steps in constructing and utilizing a NN model. Initially, the input and output parameters are defined based on the problem requirements. Following this, data are entered for training and validation purposes to ensure the model can learn and generalize effectively. Next, an appropriate NN model structure is determined, including factors like the number of layers and neurons. The model is then trained using the provided data, and its performance is validated against the validation dataset. If the obtained results are satisfactory, the process progresses to the creation of a Simulink of the model. However, if the results are not satisfactory, the process returns to the model training step, allowing for modifications to the number of layers and neurons to optimize the model's accuracy and performance.

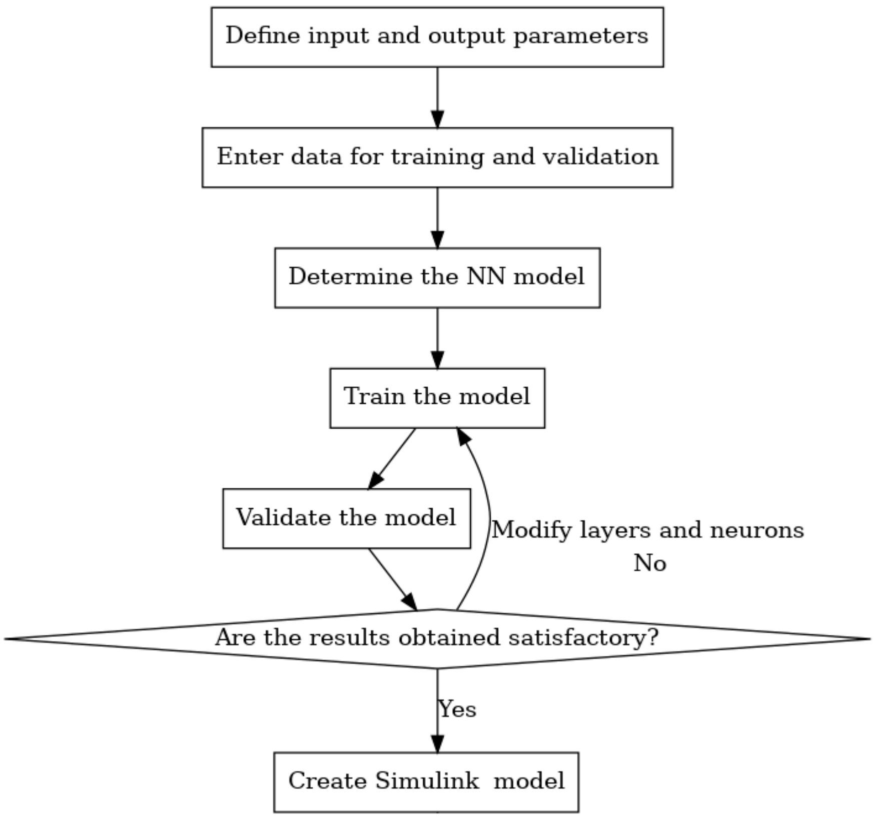

Figure 5. Basic flowchart of NN.

Consequently, the ability of NNs to deliver practical, fast, reliable solutions and robust accuracy and performance has increased their adoption in lots of engineering disciplines and their potential for sophisticated engineering applications [37,50–52].

3. Results and Discussion

3.1. Experimental Results

The LL value of the unreinforced clay was 45.00%, whereas in the reinforced samples, the LL values ranged from 38.80% to 42.30%. The minimum LL value was determined in the K + 2.0% BF sample, while the maximum LL value was in the K + 3.0% BF sample.

The PL value of the unreinforced clay was 24.00%, while in the reinforced samples, the PL value ranged from 26.00% to 28.00%. The minimum PL value was determined in the K + 3.0% BF sample, while the maximum PL value was in the K + 2.0% BF sample.

The PI value of the unreinforced clay was 21.00%, while the PI values of the reinforced samples ranged from 10.80% to 16.30%. The minimum PI value was determined in the K + 2.0% BF sample, while the maximum PI value was in the K + 3.0% BF sample.

It was determined that the LL values of the reinforced samples decreased by 6.00% to 13.78% compared to the unreinforced clay sample. The PL values increased by 8.33% to 16.67%, and the PI values decreased by 22.38% to 48.57% (Table 4).

Table 4. Changes in LL, PL, PI, and q_u values of reinforced samples compared to unreinforced clay.

Samples	LL (% Change)	PL (% Change)	PI (% Change)	q_u (% Change)
K + 1.0% BF	−10.00	10.00	−32.86	161.14
K + 1.5% BF	−10.67	15.42	−40.48	181.93
K + 2.0% BF	−13.78	16.67	−48.57	222.72
K + 2.5% BF	−12.22	14.21	−42.43	207.94
K + 3.0% BF	−6.00	8.33	−22.38	172.30

(−): Indicates a decrease in values.

After BF reinforcement, the LL values of the soil decreased due to the water absorption properties of the fiber, making the soil more stable [27]. This reduction in the LL is attributed to the conversion of static forces in the BF into frictional forces due to impacts during the LL test. As a result, the soil became more resistant to shear and flow [26,29]. The decrease in the LL values of the BF-reinforced samples led to a reduction in the soil plasticity, resulting in a soil with higher strength [53].

The q_u value of the unreinforced clay was found to be 294.08 kPa [21]. In this study, the unconfined compression tests conducted on samples reinforced with 1.0%, 1.5%, 2.0%, 2.5%, and 3.0% BF resulted in q_u values of 767.95 kPa, 829.11 kPa, 949.06 kPa, 905.60 kPa, and 800.77 kPa, respectively (Table 3). The addition of BF resulted in an increase in the q_u values of the samples in all mixtures. However, after the 2.0% BF reinforcement, the q_u values decreased slightly (Figure 6). The q_u values of the reinforced samples increased by 161.14% to 222.72% compared to the q_u value of the unreinforced clay (Table 4).

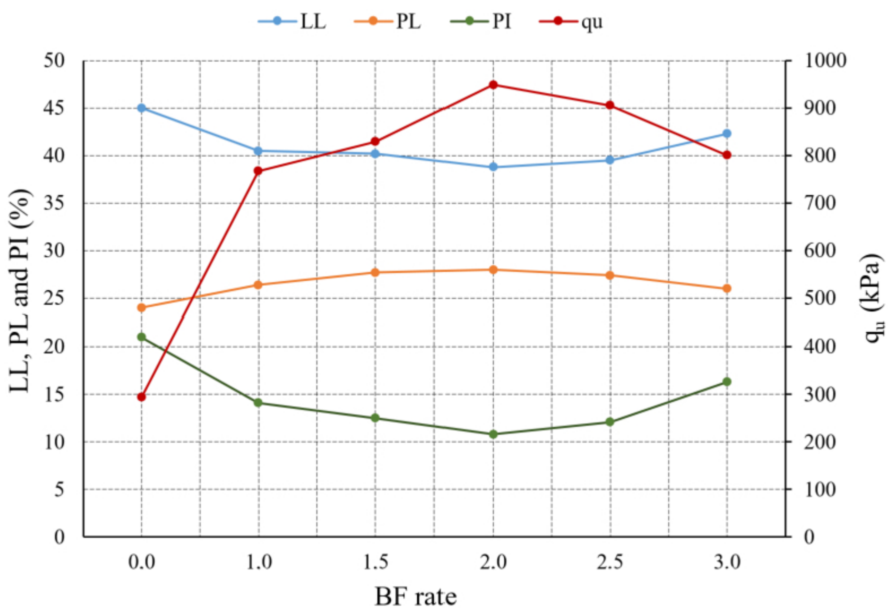

Figure 6. Changes in the LL, PL, PI, and q_u values of the soil depending on the BF ratio.

The decrease in strength with an increasing fiber ratio was explained by Gao et al. [18] as follows: As the BF content increases, the interaction between the fibers and the soil intensifies. However, the frictional resistance between the fibers is significantly lower than the surface forces between the fibers and soil particles. This makes it difficult for external forces to convert into internal fiber forces in the form of surface forces, hindering the prevention of overall soil deformation. When the BF content is too high, electrostatic interactions between the fibers promote the clustering of fiber filaments within the soil sample, which complicates the even distribution of the fibers. This results in the formation of weak stress regions that are not conducive to stress transfer. Consequently, an excessive amount of fibers may reduce the reinforcing effect of the fibers.

Furthermore, with increasing fiber content, clustered fibers may not have direct contact with soil particles; hence, the bonding effect between the fibers and soil weakens. An excessive fiber concentration tends to create a weak structural surface in the soil, leading to a decrease in the soil strength [14]. In this study, the q_u values increased up to 2.0% BF, but with further additions of BF, the strength decreased due to fiber clustering, which reduced the bonding effect between the fiber and the soil.

When the results of the experimental studies are evaluated together, it can be observed that the changes in the LL, PL, and PI values of the clay, as well as the changes in the q_u values, are consistent with the BF reinforcement ratio (Figure 6). The most crucial parameter in this alignment among the parameters was the BF reinforcement ratio. Indeed, as the BF ratio increased, there was an increase in the q_u and PL values, while the LL and PI values started to decrease. Upon reaching the 2.0% BF ratio, both the q_u and PL values reached their maximum, while the LL and PI values reached their minimum values at this BF ratio. With the BF ratio exceeding 2.0%, decreases in the q_u and PL values and increases in the LL and PI values began.

3.2. Simulation Results

In this study, experimental tests were conducted to determine the proportions of BF and K corresponding to each LL, PL, and q_u value. These proportions were stored in lookup tables for use in the NN model.

The LL, PL, and q_u values obtained from the experimental study were the input data for the NN model used in this research. The BF and K proportions were designated as the output data of the NN model. Thus, the NN model employed in this study was a one-input, two-output system. The outputs of the NN model were BF and K, while the input was either the q_u, LL, or PL. The number of hidden neurons was determined through a trial-and-error approach and set to five. The structure of the NN model used in this study is presented in Figure 7.

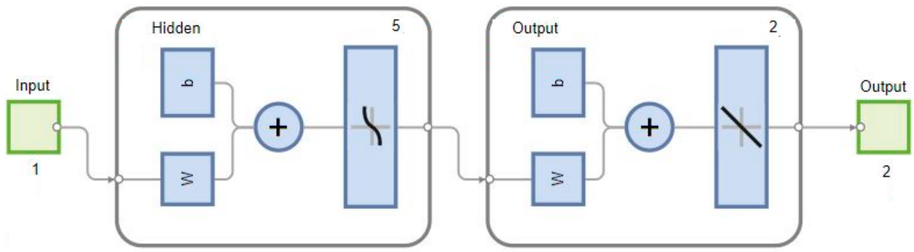

Figure 7. The structure of the NN model used in this study.

A total of 30 data were utilized in this study. Among these, 20 data were used for training, while 5 data each were allocated for validation and testing. Thus, the data were distributed for training, validation, and testing at 70%, 15%, and 15%, respectively.

Separate NN models were developed in the Matlab/Simulink Environment based on the values of LL, PL, and q_u. In each of the developed NN models, the appropriate output values for the BF and K proportions were predicted based on the input values. The Simulink block diagrams that generated outputs for the sample input values for each NN model are presented in Figures 8–10.

The diagram shown in Figure 8 represents the NN model that predicted the appropriate BF and K proportions based on the LL input value. Upon examining the model, for a LL value of 38.8%, the corresponding proportions of K and BF were determined to be 97.78% and 2.216%, respectively.

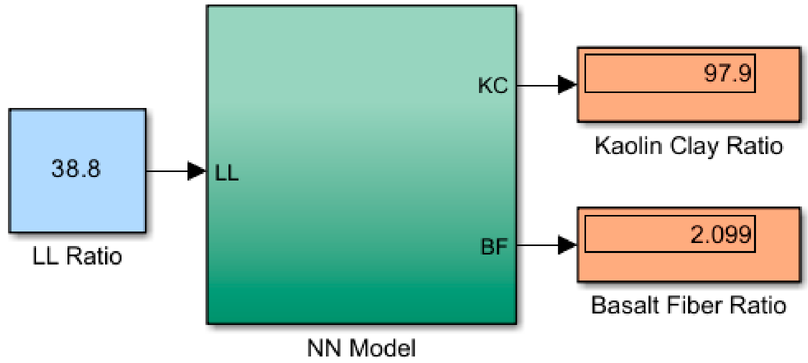

Figure 8. ANN results of LL.

The diagram shown in Figure 9 illustrates the NN model that predicted the appropriate BF and K proportions based on the PL input value. In the model output, for a given PL value of 28%, the corresponding proportions of K and BF were determined to be 98.03% and 1.963%, respectively.

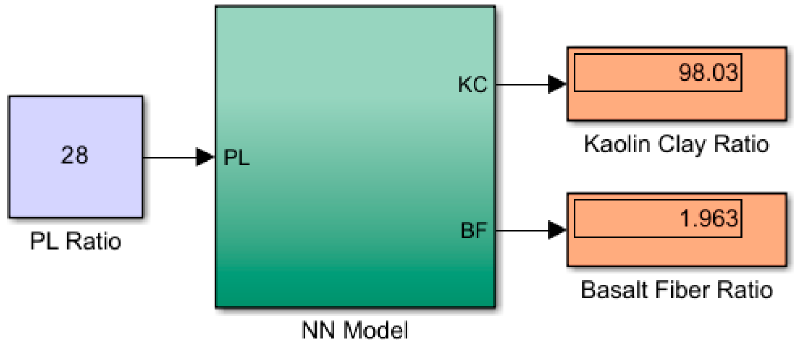

Figure 9. ANN results of PL.

Figure 10 presents the NN model that predicted the appropriate BF and K proportions based on the q_u value. For a q_u value of 949.06 kPa, the model predicted that the mixture should contain 99.96% K and 2.043% BF.

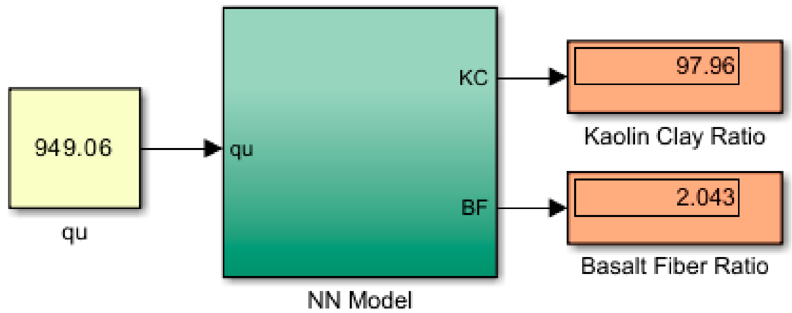

Figure 10. ANN results of q_u.

To examine the performance of the NN model used in this study, the actual values obtained from experimental studies were compared with the predicted values generated by the NN model. The examples are presented in Table 5. The appropriateness of the prediction outputs generated by the NN model with the actual results obtained experimentally is shown in Table 3. In Table 3, the rows highlighted in bold represent the data used in the Simulink diagrams shown in Figures 8–10. It can be observed that all three models predicted results very close to the experimental data.

Table 5. Comparison of experimental and ANN outputs.

Inputs	Sample		Experimental Outputs		ANN Outputs	
			K Ratio (%)	BF Ratio (%)	K Ratio (%)	BF Ratio (%)
LL (%)	1	45.00	100	0	100.00	00.00
	2	40.50	99	1.0	97.84	2.161
	3	**38.80**	**98.0**	**2.0**	**97.90**	**2.099**
	4	39.50	97.5	2.5	97.78	2.216
PL (%)	1	24.00	100	0	100.00	00.00
	2	26.40	99.0	1.0	98.98	1.023
	3	**28.00**	**98.0**	**2.0**	**98.03**	**1.963**
	4	27.41	97.5	2.5	97.37	2.629
q_u (kPa)	1	294.08	100	0	100.00	00.00
	2	797.95	99	1.0	97.68	2.324
	3	**949.06**	**98.0**	**2.0**	**97.96**	**2.043**
	4	905.60	97.5	2.5	97.93	2.074

However, it is important to note that the deviations observed, especially at lower BF ratios, were primarily due to the limited representation of lower BF ratios in the dataset used to train the NN model. As a result, the model's generalization capability in this range may be slightly reduced.

As shown in Table 5, when the BF ratio is 2%, the values obtained from the experimental data are in complete agreement with the results predicted by the NN model. In cases where the BF ratio is less than or greater than 2%, some deviations are observed between the experimental and NN model results. These deviations do not significantly detract from the overall validity of the NN model and highlight areas for future improvement in model training datasets.

In this study, the Levenberg–Marquardt algorithm was employed, and the regression coefficient (R) was calculated as 0.99 for each tree model. The proximity of the R value to 1 indicates that the model's output closely aligns with the actual values. The regression curves of the model are presented in Figure 11 for verification.

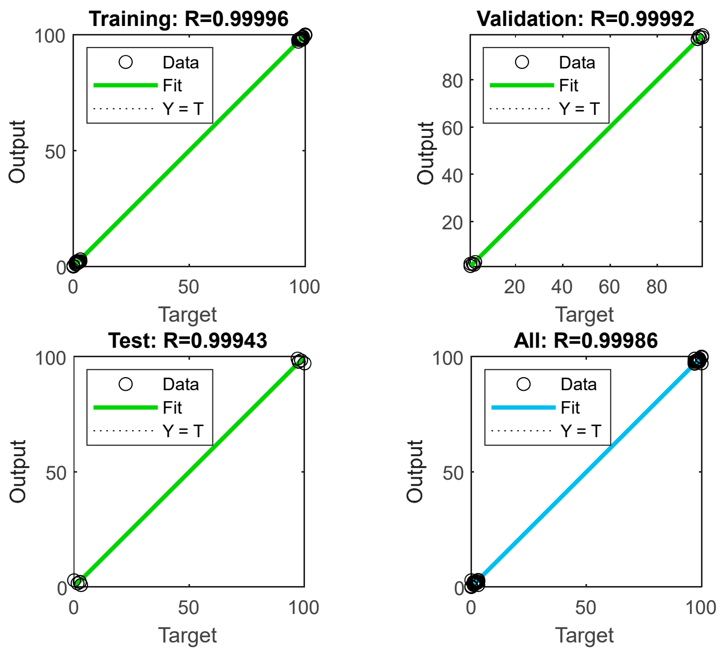

Figure 11. The regression curves of the model.

Finally, to ensure that the ANN model was not overfitted or underfitted during the training phase, the model was tested using data that were not used in the training process. The experimental data used for testing were not included in the training or validation phases, ensuring the independence of the test set. As a result of the test, the R and RMSE values were found to be 0.99 and 0.2, respectively. The regression curve corresponding to the NN model with the LL input is presented in Figure 12.

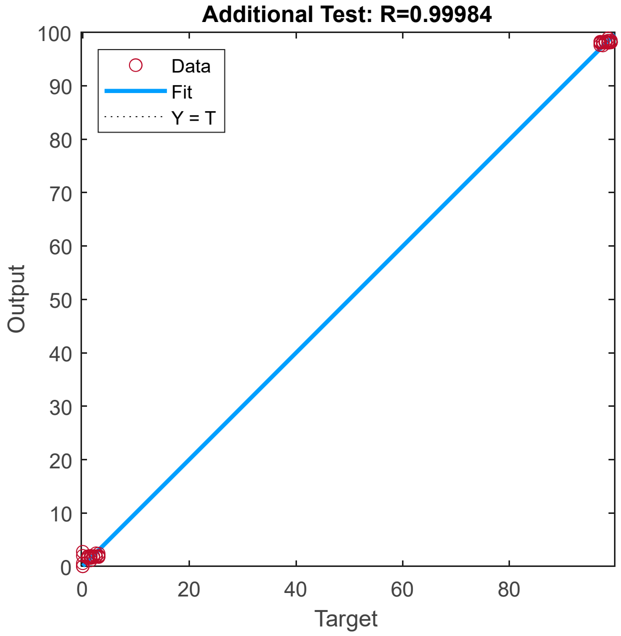

Figure 12. The test regression curve of the model.

As part of the evaluation process, a 5-fold cross-validation method was used to test the reliability of the model. This method is important for evaluating models because it helps avoid overfitting, confirms the model's reliability, and checks its ability to make accurate predictions based on new data [46,47]. In this process, the dataset was divided into five parts. The model was trained on four parts and tested on the remaining one. This was repeated five times so that each part was used for testing once, making the evaluation more reliable and consistent.

In this study, the performance and reliability of the model were assessed by comparing it with other AI methods, such as GPR, ensemble, SVM, LR, and DT, using the 5-fold cross-validation method.

The performance metrics are illustrated in Figure 13 as a radar chart, providing a visual comparison of the NN model with other AI methods, including the LR, SVM, DT, GPR, and Ensemble methods. Specifically, the NN model achieved the lowest RMSE value of 0.44936, indicating the smallest error between the predicted and experimental outputs. Moreover, the NN model exhibited the highest correlation coefficient (R = 0.82), suggesting an agreement between the predicted and experimental results.

In contrast, other models, such as the LR, SVM, DT, GPR, and Ensemble methods, showed higher RMSE values, ranging from 0.53925 to 0.57154, and lower R values, ranging from 0.68 to 0.72. These findings highlight the better predictive accuracy and reliability of the NN model in this study.

In the radar chart, the values increase from the inner point to the outer. Compared to the other methods, since the R value of the NN is closest to 1, it is in the outer ring of the radar chart, and since its RMSE value is the lowest, it is in the inner ring compared to the others.

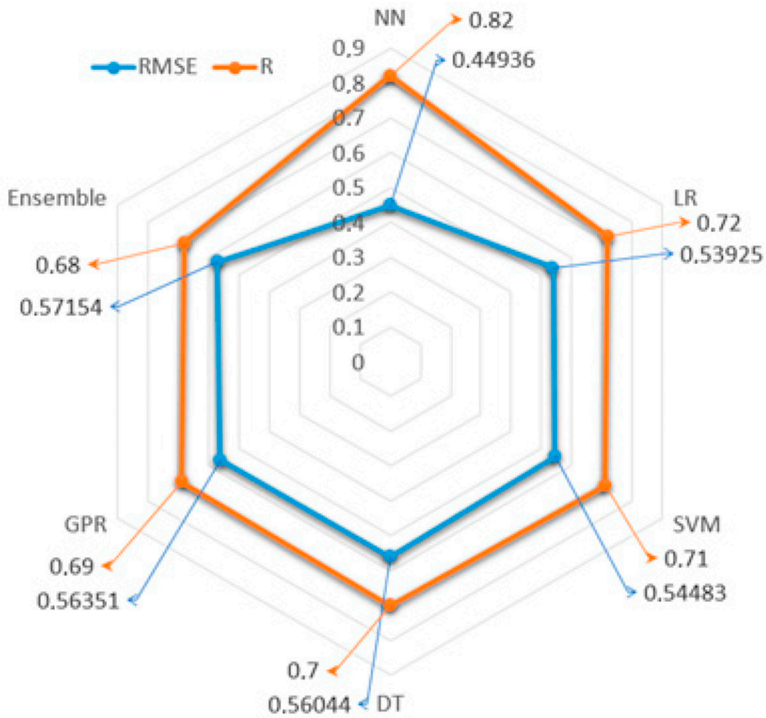

Figure 13. R and RMSE values of different AI techniques obtained from cross-validation.

4. Conclusions

In this study, 12 mm long BF was used as a reinforcement material in K at different ratios, and LL, PL, and unconfined compression tests were conducted to investigate the changes in the LL, PL, PI, and q_u values of the soil due to BF reinforcement. The experimental results obtained from these tests were used as input data for an AI model. This study aimed to identify the proportions of K and BF by considering the LL, PL, and q_u values. The effects of different BF ratios on soil behavior were evaluated, and the most suitable mixture ratios were determined. Additionally, the accuracy and predictive capability of the NN model were demonstrated, highlighting the effective application of AI methods in geotechnical engineering and materials. In summary, this study successfully combined experimental and analytical approaches to provide a practical solution.

It offers a practical tool for predicting the optimal BF ratio to achieve desired soil properties, eliminating the need for labor-intensive experiments. It also contributes to sustainable engineering practices by promoting the use of BF, a naturally abundant and environmentally friendly material, as a reinforcement agent. Moreover, this study demonstrates the potential of integrating artificial intelligence into geotechnical engineering.

In this study, low-plasticity K was selected as the soil type to be reinforced, and 12 mm long BF was used in various proportions. Therefore, it should be noted that the optimum fiber ratio determined in this study is applicable to low-plasticity clays but may not be suitable for different soil types. In the future, studies focusing on the use of BF with varying lengths and proportions in different soil types are necessary.

Similarly, the NN model developed in this study is also specific to the low-plasticity kaolin clay used in the experiments, and its applicability to other soil types requires further investigation. Additionally, the model's accuracy is contingent on the quality and quantity of the experimental data used for training, meaning that a limited dataset could restrict its generalization capability. Moreover, the effectiveness and robustness of the NN model were assessed through 5-fold cross-validation and benchmarked against other AI techniques, including the LR, SVM, DT, GPR, and Ensemble methods. The ANN model exhibited exceptional predictive performance, attaining the highest correlation coefficient (R = 0.82) and surpassing the other models in both precision and dependability.

Additionally, the data obtained from this study will contribute to the literature on the use of BF, which is naturally abundant and produced from basalt rock, as an eco-friendly and sustainable reinforcement material in soil stabilization applications.

Although the use of BF in engineering applications is becoming increasingly common, it also has significant limitations. One of the most important limitations is the need for different BF proportions in different soil types. Therefore, it is necessary to determine the optimum BF ratio based on the soil type. Another important limitation is the application depth in BF reinforcement studies. While it is easier to use in fill soils, applying this reinforcement technique to deeper soils is more challenging. To implement this application, it is necessary to conduct studies requiring equipment and qualified personnel, such as those involved deep mixing methods.

Author Contributions: Y.A.T., Z.B.D., Z.G. and H.G. wrote the main manuscript text and prepared all figures and tables. All authors have read and agreed to the published version of the manuscript.

Funding: This study was financially supported by the Scientific Research Projects Coordination Unit of Firat University (FÜBAP) under project number MF.24.122.

Data Availability Statement: The original contributions presented in the study are included in the article. Further inquiries can be directed to the corresponding author.

Conflicts of Interest: The authors declare no conflicts of interest.

References

1. Karthik, K.; Unnam, N.K.; Thamilarasan, J.; Kolappan, S.; Rameshkumar, R. Design and Analysis of Cantilever Beam Used Kevlar Fiber Composite for Automobile Applications. *Mater. Today Proc.* **2022**, *59*, 1817–1823. [CrossRef]
2. Ramesh, V.; Karthik, K.; Cep, R.; Elangovan, M. Influence of Stacking Sequence on Mechanical Properties of Basalt/Ramie Biodegradable Hybrid Polymer Composites. *Polymers* **2023**, *15*, 985. [CrossRef] [PubMed]
3. Murali, B.; Karthik, K.; Marotrao, S.S.; Laxmaiah, G.; Yadav, A.S.; Prasanth, I.S.N.V.R.; Abbas, M. Mechanical and dynamic mechanical properties of hybrid kevlar/natural fiber composites. *Mater. Res. Express* **2023**, *10*, 105305.
4. Tang, C.; Shi, B.; Gao, W.; Chen, F.; Cai, Y. Strength and Mechanical Behavior of Short Polypropylene Fiber Reinforced and Cement Stabilized Clayey Soil. *Geotext. Geomembr.* **2007**, *25*, 194–202. [CrossRef]
5. Abdi, M.R.; Parsapajouh, A.; Arjomand, M.A. Effects of Random Fiber Inclusion on Consolidation, Hydraulic Conductivity, Swelling, Shrinkage Limit and Desiccation Cracking of Clays. *Int. J. Civ. Eng.* **2008**, *6*, 284–292.
6. Ahmad, F.; Bateni, F.; Azmi, M. Performance Evaluation of Silty Sand Reinforced with Fibres. *Geotext. Geomembr.* **2010**, *28*, 93–99. [CrossRef]
7. Diambra, A.; Ibraim, E.; Wood, D.M.; Russell, A.R. Fibre Reinforced Sands: Experiments and Modeling. *Geotext. Geomembr.* **2010**, *28*, 238–250.
8. Zaimoglu, A.S. Freezing–Thawing Behavior of Fine-Grained Soils Reinforced with Polypropylene Fibers. *Cold Reg. Sci. Technol.* **2010**, *60*, 63–65. [CrossRef]
9. Estabragh, A.R.; Bordbar, A.T.; Javadi, A.A. Mechanical Behavior of a Clay Soil Reinforced with Nylon Fibers. *Geotech. Geol. Eng.* **2011**, *29*, 899–908. [CrossRef]
10. Kinjal, S.; Desai, A.K.; Solanki, C.H. Experimental Study on the Atterberg Limits of Expansive Soil Reinforced with Polyester Triangular Fibers. *Int. J. Eng. Res. Appl.* **2012**, *2*, 636–639.
11. Eskişar, T.; Karakan, E.; Altun, S. Effects of Fibre Reinforcement on Liquefaction Behaviour of Poorly Graded Sands. *Procedia Eng.* **2016**, *161*, 538–542. [CrossRef]
12. Roustaei, M.; Eslami, A.; Ghazavi, M. Effects of Freeze-thaw Cycles on a Fiber Reinforced Fine Grained Soil in Relation to Geotechnical Parameters. *Cold Reg. Sci. Technol.* **2015**, *120*, 127–137. [CrossRef]
13. Cui, H.; Jin, Z.; Bao, X.; Tang, W.; Dong, B. Effect of Carbon Fiber and Nanosilica on Shear Properties of Silty Soil and The Mechanisms. *Constr. Build. Mater.* **2018**, *189*, 286–295. [CrossRef]
14. Bao, X.; Huang, Y.; Jin, Z.; Xiao, X.; Tang, W.; Cui, H.; Chen, X. Experimental Investigation on Mechanical Properties of Clay Soil Reinforced with Carbon Fiber. *Constr. Build. Mater.* **2021**, *280*, 122517. [CrossRef]

15. Wang, S.; Xue, Q.; Ma, W.; Zhao, K.; Wu, Z. Experimental Study on Mechanical Properties of Fiber-Reinforced and Geopolymer-Stabilized Clay Soil. *Constr. Build. Mater.* **2021**, *272*, 121914. [CrossRef]
16. Czigány, T.; Vad, J.; Pölöskei, K. Basalt Fiber as A Reinforcement of Polymer Composites. *Period. Polytech. Mech. Eng.* **2005**, *49*, 3–14.
17. Jamshaid, H.; Mishra, R. A Green Material from Rock: Basalt Fiber-A Review. *J. Text. Inst.* **2015**, *107*, 923–937. [CrossRef]
18. Gao, L.; Hu, G.; Xu, N.; Fu, J.; Xiang, C.; Yang, C. Experimental Study on Unconfined Compressive Strength of Basalt Fiber Reinforced Clay Soil. *Adv. Mater. Sci. Eng.* **2015**, *2015*, 561293. [CrossRef]
19. Kale, R.Y.; Dahake, N.D.; Sahu, S.M.; Gawande, G.A.; Wailker, P.J.; Patekar, V.R.; Pawar, C.R. Soil Stabilization by Using Basalt Fibers. *Int. J. Sci. Res. Eng. Trends* **2020**, *6*, 1931–1935.
20. Sungur, A.; Yazıcı, M.F.; Keskin, S.N. Bazalt Lifi ile Güçlendirilmiş Killi Zeminin Mühendislik Özellikleri Üzerine Deneysel Araştırma. *Avrupa Bilim Teknol. Derg. Özel Sayı* **2021**, *28*, 895–899. [CrossRef]
21. Gürocak, Z.; Topçuoğlu, Y.A. Bazalt Fiber Kullanımının Düşük Plastisiteli Kilin Serbest Basınç Dayanımı Üzerindeki Etkisi. *Güm. Üniv. Fen Bilim. Derg.* **2023**, *13*, 688–701. [CrossRef]
22. Aslan Topçuoğlu, Y.; Gürocak, Z. Sodyum Bentonit Kilini Güçlendirmede Maksimum Dayanım için Optimum Bazalt Fiber Oranının Belirlenmesi. *Dicle Univ. J. Eng.* **2023**, *14*, 479–487.
23. Aslan Topçuoğlu, Y.; Gürocak, Z. The Effect of Basalt Fiber Reinforcement at Different Ratios on the Unconfined Compressive Strength of Kaolin. *Niğde Ömer Halisdemir Univ. J. Eng. Sci.* **2024**, *13*, 169–175. [CrossRef]
24. Ndepete, C.P.; Sert, S. Use of Basalt Fibers for Soil Improvement. *Acta Phys. Pol.* **2016**, *130*, 355–356. [CrossRef]
25. Ocakbaşı, P. Bazalt Fiber Katkısının Killi Zeminlerin Drenajsız Kayma Direncine Etkisi. Yüksek Lisans Tezi, Sakarya Üniversitesi, Fen Bilimleri Enstitüsü, Sakarya, Turkey, 2019.
26. Aravalli, A.B.; Hulagabali, A.M.; Solanki, C.H.; Dodagoudar, G.R. Enhancement of Index and Engineering Properties of Expansive Soil Using Chopped Basalt Fibers. In Proceedings of the Indian Geotechnical Conference 2017 GeoNEs, Guwahati, India, 14–16 December 2017; IIT Guwahati: Guwahati, India, 2017; pp. 1–4.
27. Chaudhary, R. Enhancing the Properties of Soil by Stabilization Technique Using Basalt Fiber. Master's Thesis, Civil Engineering Department, Delhi Technological Unıversity, New Delhi, India, 2021.
28. Khudhair, A.H.; Mahmood, R.A.; Jaber, M.A. Improving Some Geotechnical Properties of Cohesive Soils by Adding Basalt Fibers and Portland Cement in Basra Governorate-Southern Iraq. *Des. Eng.* **2022**, *1*, 1509–1522.
29. Mukhtar, M.; Kumar, A. To Study the Behavior of Compacted Soil Using Basalt Fibers. *Int. J. Innov. Res. Eng. Manag.* **2022**, *9*, 360–366.
30. Aishwarya, R.; Rachel, P.P. Comparative Study on Atterberg Limits of Soil and Basalt Fiber Composite as an Eco-friendly Construction Material. *Mater. Today Proc.* **2023**, *77*, 563–567. [CrossRef]
31. Armaghani, D.J.; Mirzaei, F.; Shariati, M.; Trung, N.T.; Shariati, M.; Trnavac, D. Hybrid ANN-Based Techniques in Predicting Cohesion of Sandy-Soil Combined with Fiber. *Geomech. Eng.* **2020**, *20*, 191–205.
32. Garg, A.; Bordoloi, S.; Mondal, S.; Ni, J.J.; Sreedeep, S. Investigation of Mechanical Factor of Soil Reinforced with Four Types of Fibers: An Integrated Experimental and Extreme Learning Machine Approach. *J. Nat. Fibers* **2020**, *17*, 650–664. [CrossRef]
33. Tiwari, N.; Satyam, N. Coupling Effect of Pond Ash and Polypropylene Fiber on Strength and Durability of Expansive Soil Subgrades: An Integrated Experimental and Machine Learning Approach. *J. Rock Mech. Geotech. Eng.* **2021**, *13*, 1101–1112. [CrossRef]
34. Gul, N.; Mir, B.A. Parametric Study of Glass Fiber Reinforced Fine-grained Soil with Emphasis on Microstructural Analysis. *Int. J. Geotech. Eng.* **2022**, *16*, 716–728. [CrossRef]
35. Sungur, A.; Keskin, N. Prediction of The Shear Strength of Glass Fiber-Reinforced Clay Soil by Adaptive Neuro-Fuzzy Inference System (ANFIS). *El-Cezeri* **2022**, *9*, 1255–1264.
36. Sert, S.; Arslan, E.; Ocakbaşı, P.; Ekinci, E.; Garip, Z.; Özocak, A.; Bol, E.; Ndepete, C.P. Stabilization of Expansive Clays with Basalt Fibers and Prediction of Strength by Machine Learning. *Arab. J. Sci. Eng.* **2024**, *49*, 13651–13670. [CrossRef]
37. Aslan Topçuoğlu, Y.; Duranay, Z.B.; Gürocak, Z. Evaluation of the Changes in the Strength of Clay Reinforced with Basalt Fiber Using Artificial Neural Network Model. *Appl. Sci.* **2024**, *14*, 10362. [CrossRef]
38. Li, Z.; Ma, J.; Ma, H.; Xu, X. Properties and applications of basalt fiber and its composites. *IOP Conf. Ser. Earth Environ. Sci.* **2018**, *186*, 012052. [CrossRef]
39. Militky, J.; Kovacic, V. Ultimate Mechanical Properties of Basalt Filaments. *Text. Res. J.* **1996**, *66*, 225–229. [CrossRef]
40. Wei, B.; Cao, H.; Song, S. Surface Modification and Characterization of Basalt Fibers with Hybrid Sizings. *Compos. Part A: Appl. Sci. Manuf.* **2011**, *42*, 22–29. [CrossRef]
41. *ASTM D4318-17e1*; Standard Test Methods for Liquid Limit, Plastic Limit, and Plasticity Index of Soils. ASTM International: West Conshohocken, PA, USA, 2017.
42. *ASTM D698-12e2*; Standard Test Methods for Laboratory Compaction Characteristics of Soil Using Standard Effort. ASTM International: West Conshohocken, PA, USA, 2012.

43. *ASTM D2166M-16*; Standard Test Method for Unconfined Compressive Strength of Cohesive Soil. ASTM International: West Conshohocken, PA, USA, 2016.
44. Guldemir, H.; Sengur, A. Online Modulation Recognition of Analog Communication Signals Using Neural Network. *Expert Syst. Appl.* **2007**, *33*, 206–214. [CrossRef]
45. Duranay, Z.B.; Guldemir, H. Fuzzy Logic Based Selective Harmonic Elimination for Single Phase Inverters. *Adv. Sci. Technol. Eng. Syst. J.* **2018**, *3*, 161–167. [CrossRef]
46. Aliser, A.; Duranay, Z.B. Fire/Flame Detection with Attention-Based Deep Semantic Segmentation. *Iran. J. Sci. Technol. Trans. Electr. Eng.* **2024**, *48*, 705–717. [CrossRef]
47. Guldemir, N.H.; Alkan, A. Classification of Optical Coherence Tomography Images Via Deep Learning. *Firat Univ. J. Eng. Sci.* **2021**, *33*, 607–615.
48. Duranay, Z.B.; Guldemir, H. Extreme Learning Machine Based Selected Harmonic Elimination for Single Phase Inverters. *Measurement* **2019**, *131*, 300–308. [CrossRef]
49. Uyanık, H.; Ozcelik, S.T.A.; Duranay, Z.B.; Sengur, A.; Acharya, U.R. Use of Differential Entropy for Automated Emotion Recognition in a Virtual Reality Environment with EEG Signals. *Diagnostics* **2022**, *12*, 2508. [CrossRef] [PubMed]
50. Duranay, Z.B. Neural Network Based Harmonic Elimination in Single-Phase Inverters. *COMPEL-Int. J. Comput. Math. Electr. Electron. Eng.* **2023**, *42*, 543–564. [CrossRef]
51. Demir, T.; Duranay, Z.B.; Demirel, B.; Yildirim, B. Artificial Neural Network Evaluation of Concrete Performance Exposed to Elevated Temperature with Destructive–Non-Destructive Tests. *Neural Comput. Appl.* **2024**, *36*, 17079–17093. [CrossRef]
52. Gürocak, Z.; Solanki, P.; Alemdag, S.; Zaman, M.M. New considerations for empirical estimation of tensile strength of rocks. *Eng. Geol.* **2012**, *145*, 1–8. [CrossRef]
53. Bian, X.; Zeng, L.; Ji, F.; Xie, M.; Hong, Z. Plasticity Role in Strength Behavior of Cement-Phosphogypsum Stabilized Soils. *J. Rock Mech. Geotech. Eng.* **2022**, *14*, 1977–1988. [CrossRef]